Nano Research

Open Access

Research Article

Performance evaluation of homogeneous dual-atom site M_2-N_6-graphene catalysts for hydrogen evolution reaction

Jing Meng[1,§], Letong Feng[1,§], Zhaoyang Zhang[1,2], Liang Zhang[2], Xiangwen Liu[3]✉, Zhenwei Zhang[4]✉, and Wenming Sun[1]✉

[1] *Department of Chemistry, Capital Normal University, Beijing 100048, China*
[2] *Dassault Systemes (Shanghai) Information Technology Co., Ltd., Shanghai 200120, China*
[3] *Institute of Analysis and Testing, Beijing Academy of Science and Technology, Beijing 100094, China*
[4] *Linyi Vocational University of Science and Technology (Linyi Branch of Steinbeis Intelligent Manufacturing Technology Transfer Center), Linyi 276000, China*
[§] *Jing Meng and Letong Feng contributed equally to this work.*

Cite this article: *Nano Research*, **2025**, *18*, 94907004. https://doi.org/10.26599/NR.2025.94907004

ABSTRACT: Using first-principles calculations, we systematically investigated the hydrogen evolution reaction (HER) potential of 27 types of homogeneous dual-atom M_2-N_6-graphene catalysts. Shared nitrogen atoms between dual metal atoms were identified as crucial adsorption sites for hydrogen atoms. Notably, we found that relying solely on the free energy of hydrogen adsorption (ΔG_{H^*}) could exclude the extremely unfavorable substrates, but may lead to misleading assessments of HER activation for substrates with modest ΔG_{H^*}. Thermodynamic activity evaluation reveals that M_2-N_6-graphene (M = Cr, Co, Ni, Cu, Os, Pt) models exhibit promising HER activities. Kinetic analysis, based on the Volmer–Tafel mechanism, determined that the hydrogen coverage and relative distance between the adsorbed hydrogen atoms in the Tafel step affect the reaction energy barrier significantly. The coverage limits depend on the reaction free energy of the non-spontaneous third hydrogen adsorption step. By integrating the kinetic metric with thermodynamic assessments, we propose that the Co_2-N_6-graphene model displays superior HER activity. We further recommend selecting one of the metal positions in M_aM_b-N_6-graphene to be Cr and excluding Cu and Ni elements during the selection of the second metal atom when designing heterogeneous M_aM_b-N_6-graphene for alkaline HER catalyst. This study establishes a convenient workflow and provides valuable insights for the rational design of efficient HER catalysts.

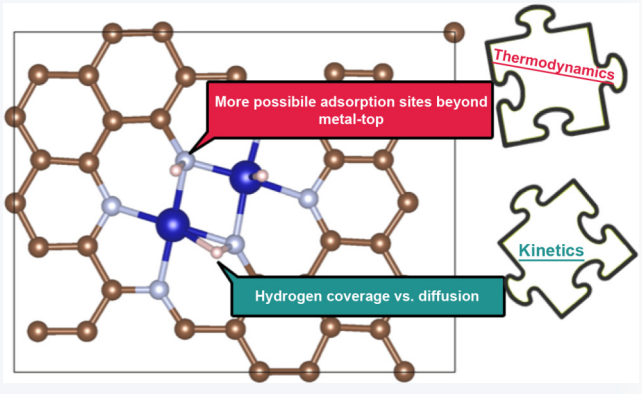

KEYWORDS: shared nitrogen site, hydrogen evolution reaction (HER), dual-atom site catalyst, M_2-N_6-graphene

1 Introduction

The transition to the low-carbon economy relies heavily on the widespread adoption of renewable energy sources, particularly hydrogen as a clean and sustainable energy carrier [1–4]. However, the efficient production of hydrogen from water electrolysis is hindered by the sluggish kinetics of hydrogen evolution reaction (HER). Conventional HER catalysts, such as platinum and its alloys, generally suffer from limitations, including high cost and scarcity. As a result, designing cheap HER catalysts with improved performance, durability and sustainability is essential to overcome the current limitations [5–9]. Developing efficient and cost-effective catalysts with tailored properties, such as enhanced surface area, tunable electronic structure and improved durability, is crucial for the widespread adoption of hydrogen energy [10–13]. To activate every metal atom in supported catalysts, shrinking the size of supported catalysts from cluster to atomic level single-atom or dual-atom sites will be the ultimate goal [14–17].

Dual-atom site catalysts (DACs), as an extension of single-atom site catalysts (SACs), not only inherit the high atom utilization

Received: July 22, 2024; **Revised:** August 20, 2024
Accepted: August 24, 2024

✉Address correspondence to Xiangwen Liu, liuxiangwen@bcpca.ac.cn; Zhenwei Zhang, zhangzhenwei@lyvust.edu.cn; Wenming Sun, swm@mail.sdu.edu.cn

efficiency of SACs, but also exhibit significant synergistic effects and tunability [18–24]. For instance, the dual-single-atom, as a parasite of Ru nanoparticle crystals, plays a pivotal role in enhancing the catalytic efficiency of the hydrogen oxidation reaction (HOR) in the Ru composite catalyst [25]. Based on the interaction between dual metals, DACs could be categorized as isolated dual single-atom configuration, N/O-bridged dual metal interaction and direct metal-metal bonding interaction [26]. Among them, the N/O-bridged dual metal interaction is a promising candidate for modulating the electronic and geometric structures of DACs. For example, Ni-Ni embedded in N-doped carbon catalysts with N-bridged Ni_2 sites have shown high activity for the reduction of CO_2 to CO [27]. Similarly, different Fe_2-N_6 configurations were obtained by changing the pyrolysis atmosphere and the N-bridged Fe_2 sites could promote CO desorption [28].

The design of novel dual-atom catalysts for HER involves a multidisciplinary strategy that combines advanced computational screening, atomic-precision synthesis techniques and electrochemical characterization. In the framework of materials genome engineering, the process can begin with computational screening of metal atoms and their combinations to identify optimal configurations that exhibit enhanced HER activity [29]. Generally, density functional theory (DFT) calculations are employed to predict the adsorption strength of hydrogen as well as its thermodynamic properties. The most promising candidates are then synthesized. The resulting materials are then characterized using techniques like X-ray photoelectron spectroscopy and scanning tunneling microscopy to confirm the existence of dual metal atoms. The electrochemical performance of the catalysts is evaluated using methods like cyclic voltammetry and chronoamperometry and the results are compared to those of conventional HER catalysts. By systematically optimizing the composition and structure of single-atom and dual-atom catalysts, it is possible to achieve significant enhancements in HER activity, stability and durability, ultimately enabling the development of more efficient and sustainable hydrogen production technologies. For example, Kumar et al. investigated the synergistic interaction at the NiCo-single-atom-dimer atomic interface based on a systematic first-principle screening [30]. Zhang and his coworkers construct a materials genome containing 26 homonuclear and 253 heteronuclear BACs (M_2/g-CN and M_IM_{II}/g-CN), where BACs represents Bi-atomic catalysts, g-CN represents graphitic carbon nitride and M_I and M_{II} represent two different metallic elements [31]. From a computational perspective, CN-based single or dual metal site catalyst models are relatively simple. Due to their significant tunability, it is easy to construct structure–property relationships with affordable computational cost [16]. However, there are two problems in computational high-throughput screening. Generally, only the hydrogen adsorption reaction free energy is considered as the sole descriptor based on the computational hydrogen electron [32]. The main steps of HER can vary depending on the pH of the solution and undergo successive Volmer step to Tafel/Heyrovsky step. Understanding these steps is crucial for designing efficient catalysts for the HER, as each step involves different thermodynamic and kinetic requirements that can be optimized for better performance. The single thermodynamic descriptor would not be sufficient. Furthermore, in such CN-based single or dual metal site catalyst models, metal top or metal-metal bridge sites are generally considered as the adsorption sites for intermediates in HER or oxygen evolution reaction (OER). However, the surrounding carbon or nitrogen sites might also act as the adsorption sites. In 2018, Fei et al. determined the carbon close to nitrogen in single-atom Ni-N-graphene catalysts acted as the adsorption sites for O* and OH* [33]. Recently, we and collaborators determined that the metal-metal shared nitrogen sites are important sites for hydrogen adsorption, which are dominant in the hydrogenation reaction [34]. In addition, we determined that Fe-V shared nitrogen sites are the HER active center, while the presence of neighboring V site shifts the pz (where orbits extending along the *z* axis are labeled as pz orbits) center of the bridging N atoms positively and intensifies the electronic spin and 3d orbital of Fe atoms, which optimizes the interaction of the H/O-containing reactant/intermediate on N and Fe sites [35]. Consequently, more hydrogen adsorption sites, especially the metal-metal shared nitrogen sites should be included when evaluating HER performance.

In this work, we constructed a workflow containing both thermodynamic and kinetic descriptors and revealed that the shared nitrogen atoms between dual metal atoms can serve as crucial adsorption sites for hydrogen. Significantly, we found that relying solely on the free energy of hydrogen adsorption can lead to misleading assessments of HER performance in high-throughput screening.

2 Computational model and details

A typical M_2-N_6-graphene slab model with 46 atoms was selected. Transition metal elements except Tc were considered (Fig. 1(a)). The lattice parameters along *x* and *y* directions are 12.824 and 9.859 Å, respectively. All atoms were allowed to relax without any constraints during optimization. A vacuum of 20 Å was set along the out-plane direction to avoid the interaction between neighboring images. In Quantum ESPRESSO suite [36, 37], generalized gradient approximation (GGA) with Perdew–Burke–Ernzerhof (PBE) functional [38] was adopted to describe exchange-correlation potential. GBRV ultrasoft pseudopotential libraries (version all_pbe_UPF_v1.5) [39] were selected. The Hubbard correction (DFT + *U*) [40] was applied for

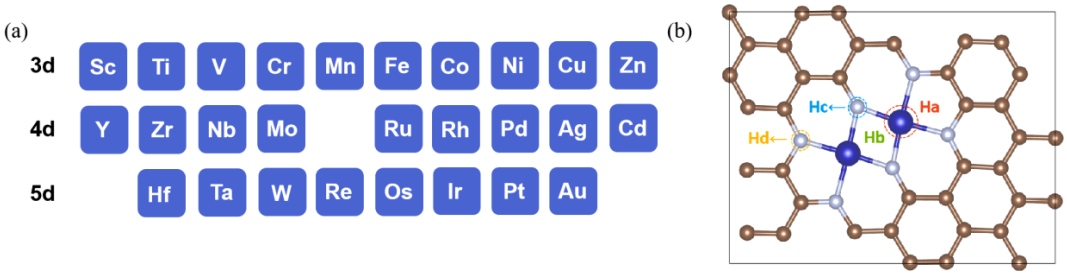

Figure 1 (a) Metal elements considered to construct M_2-N_6-graphene slab model in this work. (b) Top view of the M_2-N_6-graphene slab model as well as the adsorption sites for hydrogen.

models containing 3d metals. Spin polarization is considered. Meanwhile, in this work, the Hubbard U values were adopted from the previous high-throughput computational screening in similar single atom M-N-graphene models [41]. Since the delocalization of 4d and 5d metals were stronger than that of 3d metals, DFT + U was not applied in models with 4d and 5d metal elements. Kinetic energy and charge density cutoffs were 40 and 400 Ry, respectively, with a Marzari–Vanderbilt cold smearing [42] width of 0.03 eV to speed up self-consistent field (SCF) convergence. The first Brillouin zone integration was sampled with Γ-centered 2 × 2 × 1 and 4 × 4 × 1 k-point mesh for geometry optimization and SCF calculation, respectively. The SCF tolerance was set to 1×10^{-7} Ry, while the convergence tolerances for energies and forces were set to 1×10^{-6} Ry and 1×10^{-3} Ry/Å respectively. To evaluate the kinetic properties in Tafel step and water dissociation reaction, the nudged elastic band (NEB) method was used to locate the transition state. The adsorption energy (E_{ads}) between the single hydrogen atom and substrate was defined by $\Delta E_{ads} = E_{H/sub} - 0.5E_{H^2} - E_{sub}$, where $E_{H/sub}$, E_{sub} and E_{H^2} are the total energies for the hydrogen-adsorbed substrate, clean substrate and isolated hydrogen molecules. Based on the computational hydrogen electrode [32–43], the corresponding free energy (ΔG_{H^*}) was defined by $\Delta G_{H^*} = \Delta E_{ads} + \Delta E_{ZPE} - T\Delta S$, where ΔE_{ZPE}, T and ΔS are the difference in zero-point energy, the temperature and the difference in entropy, respectively.

3 Results and discussion

3.1 The role of metal-metal shared nitrogen-top sites in HER

For 27 types of DACs, only Hf_2-N_6-graphene exhibits non-planar character mainly because of the largest atomic radii of Hf in the considered metal elements (Fig. S1 in the Electronic Supplementary Material (ESM)). Several highly symmetrical sites, including metal-top (a), metal-metal bridge (b), metal-metal shared nitrogen-top (c) and non-shared nitrogen-top (d), were considered as the potential adsorption sites on DACs as shown in Fig. 1(b) and Fig. S2 in the ESM. The corresponding adsorption energies were calculated. The most stable binding sites are shown in Fig. S3 in the ESM. Interestingly, the preferred adsorption sites exhibit regionalized characteristics, except for Hf_2-N_6-graphene. Statistical analysis of the counts of different sites as the most stable site reveals that metal top sites and metal bridge sites each show 7 times, while metal-metal shared nitrogen-top sites show 13 times as the most stable site, accounting for nearly half of the models investigated. It indicates that shared nitrogen sites play a relatively important role in the research of dual-atom site catalysts. Therefore, the hydrogen adsorption mode on the shared nitrogen sites should be emphasized in the study of HER and hydrogenation-related reactions on similar substrates [34, 35]. The non-shared nitrogen sites have never appeared as the most stable adsorption site, so hydrogen adsorption behavior on these sites will not be further investigated.

Metal-metal bridge site is preferable for the first adsorbed hydrogen at DACs containing early-transition metals. Due to their larger atomic radii of early-transition metals, these metals suffer from significant internal stress when embedded in N4 coordination surrounding. After hydrogen adsorption, the active center undergoes a significant deformation by bumping the metal atom out-plane to release the internal stress. Upon forming a bridge-adsorbed hydrogen, both metals change from a four-coordinate to a five-coordinate N4H1 configuration, thereby releasing internal stress on dual sites simultaneously. On the contrary, metal top-site adsorption can only change the coordination configuration of single metal to N4H1 five-coordinate configuration. Furthermore, the relief of internal stress accompanied with significant distortion in M_2-N_6 region lead a huge hydrogen adsorption energy.

In a previous study, Di Liberto et al. emphasized that the notion of frontier orbitals is a much more appropriate descriptor than d-band enter in SACs systems due to the d-orbital from the definition isolated metal atom could not form a band [44]. Herein, frontier molecule orbitals are plotted to reveal the selectivity of hydrogen adsorption. According to the requirements for symmetry in the formation of molecular orbitals (MOs), s orbital of hydrogen can combine with the d_{z^2} orbital of a metal atom to form a σ bond, which leads to the formation of a H–M bond (where M stands for metal atom) at the top site of the metal. Additionally, s orbital of hydrogen can combine with the p_z orbital of nitrogen to form a σ bond, which leads to the formation of a H–N bond at the nitrogen-top site. As shown in Fig. 2(a), only the highest occupied MOs (HOMO) of Os_2-N_6-graphene and V_2-N_6-graphene (Fig. S4 in the ESM) show distinct d_{z^2} characteristics, while the HOMOs of other models such as Mn_2-N_6-graphene (Fig. 2(b)), Cr_2-N_6-graphene (Fig. S5 in the ESM) and Co_2-N_6-graphene (Fig. S6 in the ESM) are primarily composed of d_{xy} or d_{yz} orbitals and does not satisfy MO formation requirements. For Pt_2-N_6-graphene models (Fig. 2(c)), Ni_2-N_6-graphene (Fig. S7 in the ESM) and Cu_2-N_6-graphene (Fig. S8 in the ESM), the d orbitals of the metal and the p orbitals at the shared nitrogen site both contribute to the HOMO, but the orientation of these orbitals still does not meet the MO formation requirements with H-1s orbital. Due to its deep d-band center of Au, the HOMO of Au_2-N_6-graphene is composed of p_z orbitals from the nitrogen and carbon atoms surrounding the Au atoms, as shown in Fig. 2(d). The relative positions between p-orbital in metal-metal shared nitrogen and d-orbital of metal in Au_2-N_6-graphene, Pt_2-N_6-graphene, Cr_2-N_6-graphene, V_2-N_6-graphene and Os_2-N_6-graphene were plotted via projected density of states as shown in Figs. S9–S12 in the ESM. The unique HOMO orbital composition of Os_2-N_6-graphene and V_2-N_6-graphene will provide new inspiration for designing hetero-M_2-N_6-graphene catalysts in the future. Particularly for V, due to its non-noble metal nature, magnetic properties, low occupation electron number on d-orbital and partial occulated d_{z^2} feature (Fig. 3), will be suitable for local electronic structure modulation. Recently, the FeV-N_6-graphene hetero dual atomic site catalyst designed and synthesized by our collaborators has shown good activity in water splitting reactions, while its shared nitrogen atom sites between Fe-V act as HER reactions center [35].

3.2 Effect of hydrogen coverage in HER performance

If the adsorption reaction free energies for the first hydrogen ($\Delta G_{H^*-1^{st}}$) in DACs are adopted as the criteria for screening, the following DACs show good HER activities with trend as Ru_2-N_6-graphene (−0.07 eV) > Au_2-N_6-graphene (+0.10 eV) > Ni_2-N_6-graphene (−0.11 eV) > Os_2-N_6-graphene (−0.12 eV) > Co_2-N_6-graphene (−0.14 eV) (Fig. S13 in the ESM).

Tafel step describes the formation of hydrogen molecule by two adsorbed hydrogen atoms bonding together. $\Delta G_{H^*-1^{st}}$ is suitable to access to evaluate the HER activity of pure metal surface, since the

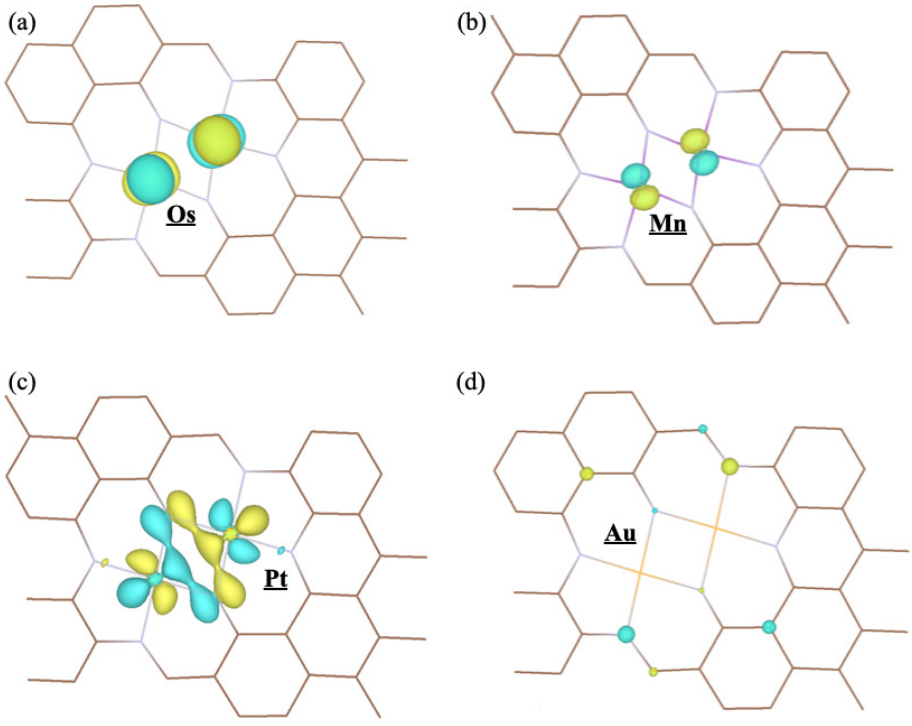

Figure 2 Highest occupied molecular orbitals for (a) Os_2-N_6-graphene, (b) Mn_2-N_6-graphene, (c) Pt_2-N_6-graphene, and (d) Au_2-N_6-graphene. The isosurface level is 0.005 a.u./Å^3.

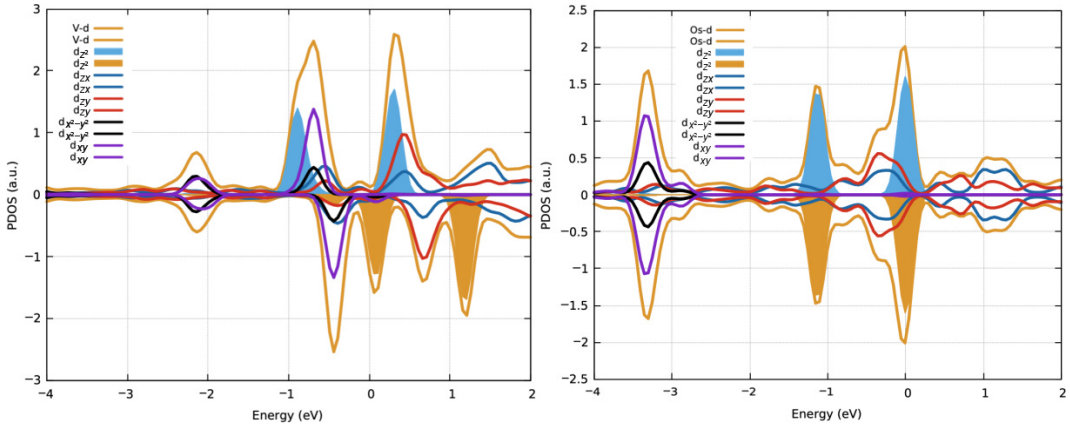

Figure 3 Projected density of states for d-band of metal V (left graph) and Os (right graph) in V_2-N_6-graphene and Os_2-N_6-graphene, respectively.

1st and 2nd hydrogen adsorption sites are equivalent. If the binding site for the second hydrogen atom is different from that of the first hydrogen atom, the case of desorption for the second hydrogen atom is no longer the same as that of the first one. Therefore, evaluating only the ΔG_{H^*-1st} may be insufficient. In this context, it is necessary to calculate the adsorption of the 2nd hydrogen atom based on the most stable configuration of the 1st hydrogen adsorption. By comparing the total energy of the adsorption configuration of hydrogen atoms at each site (metal-top, metal-metal bridge, metal-metal shared nitrogen-top), the most stable adsorption configuration of 1st and 2nd hydrogen atoms can be selected for each system, as shown in Fig. S14 in the ESM. It can be seen that for M_2-N_6-graphene models with metal M as Ti, V, Zr, Nb, Mo, Ru, Hf, Ta, W, Re and Os, the 2nd hydrogen atom adsorbs at the metal top site as the most stable configuration. For M_2-N_6-graphene models with metal M as Sc, Cr, Mn, Fe, Co, Ni, Cu, Zn, Y, Rh, Pd, Ag, Cd, Ir, Pt and Au, the 2nd hydrogen atom adsorbs at the shared nitrogen-top site as the most stable configuration.

At this point, only the metal top site and the shared nitrogen-top site act as the most stable adsorption site for 2nd hydrogen. It is easy to understand since the metal-metal bridge site is located in the center between two metal top sites or two shared nitrogen sites, so regardless of whether the 1st hydrogen atom has a preference for occupying the metal top site or the shared nitrogen-top site, the strong spatial positional effect prevents the second hydrogen atom from occupying the bridge site. Cd_2-N_6-graphene and Ag_2-N_6-graphene undergo significant deformation after the 2nd hydrogen adsorption step, indicating their poor stability.

Similarly, the ΔG_{H^*-2nd} is also evaluated. It is found that Cr_2-N_6-graphene has the reaction free energy closest to 0 eV, exhibiting exceptional HER catalytic activity, as shown in Fig. S15 in the ESM. Additionally, Ni_2-N_6-graphene (0.05 eV), Pd_2-N_6-graphene (0.13 eV), Co_2-N_6-graphene (0.11 eV), Os_2-N_6-graphene (0.11 eV), Zn_2-N_6-graphene (0.13 eV) and Pt_2-N_6-graphene (0.19 eV) have reaction free energies close to 0 eV, indicating good activity for 2nd

hydrogen on these catalysts. It is interesting to observe that Ru_2-N_6-graphene shows good HER activity in the first step but poor performance in the second step, so it is hypothesized that Ru_2-N_6-graphene may only display good HER activity under basic conditions through the Volmer–Heyrovsky mechanism, instead of via Volmer–Tafel mechanism.

Adopting ΔG_{H^*-2nd} as an evaluation criterion is based on the following assumption: The 1st hydrogen's bonding with the active center is too strong or too weak to complete Volmer efficiently, so the 2nd hydrogen, with a reaction free energy closer to 0 eV, is used as the HER intermediate. For example, in the Pd_2-N_6-graphene model, the reaction free energy for the first hydrogen is strong (−0.46 eV), but the reaction free energy for the second hydrogen is only 0.06 eV. If only the ΔG_{H^*-1st} was used to judge the HER activity of Pd_2-N_6-graphene, it would be insufficient, but as the coverage increases, the calculated results based on ΔG_{H^*-2nd} indicate that it may achieve good HER activity. A similar situation occurs with the Cr_2-N_6-graphene model, where the reaction free energy for the 2nd hydrogen is closer to 0 eV than that for the 1st hydrogen.

Till now, it can be seen that using the reaction free energy of the first adsorbed hydrogen for evaluation is very convenient for screening and excluding models with large deformation after hydrogen adsorption, such as M_2-N_6-graphene containing early transition metals (Sc, Ti, Y, Zr, Nb, Hf, Ta, W). However, the judgment for H_{1st}@M_2-N_6-graphene with modest binding strength may be insufficient. In other words, the coverage of hydrogen is crucial in HER potential screening.

In M_2-N_6-graphene model, there are one metal bridge site, two metal top sites and two shared nitrogen top sites, so a maximum of five hydrogen atoms can be occupied simultaneously on the reaction region. Based on the most stable configuration of the first two adsorbed hydrogen atoms, the adsorption modes for 3rd hydrogen were considered. From Fig. S16 in the ESM, it can be found that the 3rd hydrogen is more stable on the metal top for M_2-N_6-graphene with metals such as Sc, V, Cr, Mn, Fe, Co, Ni, Cu, Zn, Zr, Nb, Rh, Pd, Pt and Au, while the 3rd hydrogen is more stable on the shared nitrogen for M_2-N_6-graphene with metals such as Ti, Y, Mo, Ru, Hf, Ta, W, Re, Os and Ir. Similarly, according to the most stable configuration after the three hydrogen atoms adsorption, the 4th hydrogen adsorption modes were also investigated. For M_2-N_6-graphene with metals such as Cr, Mn, Fe, Co, Ni, Cu, Zn, Y, Rh, Pd, Ir, Pt and Au, the 4th hydrogen is more stable on the metal top site, while the 4th hydrogen is more stable on the shared nitrogen-top for M_2-N_6-graphene with metals such as Sc, Ti, V, Zr, Nb, Mo, Ru, Hf, Ta, W, Re and Os, as shown in Fig. S17 in the ESM.

As shown in Fig. 4, the most stable adsorption configurations of the first four hydrogen atoms are colored according to adsorption sites. Several typical adsorption configurations were exhibited in Fig. S18 in the ESM. For the first four hydrogen adsorptions, the ΔG_{H^*} was calculated for each step and the corresponding step diagram was drawn, as shown in Fig. S19 in the ESM.

The reaction free energy for the 3rd hydrogen in all models is positive, indicating non-spontaneous processes. As shown in Fig. 4, the free energy barrier required for the third hydrogen addition varies significantly. For models such as Fe_2-N_6-graphene, Ni_2-N_6-graphene, Cu_2-N_6-graphene, Mo_2-N_6-graphene, Pd_2-N_6-graphene, Hf_2-N_6-graphene, Ta_2-N_6-graphene, W_2-N_6-graphene, Re_2-N_6-graphene and Pt_2-N_6-graphene, the free energy barrier required for the third hydrogen addition is greater than 0.8 eV, making their 3rd hydrogen adsorption reaction difficult to carry out. For these models that only the 1st and 2nd hydrogen adsorption steps need to be considered.

According to the successive hydrogen adsorption steps considered, the screening process should consider both the various of adsorption sites and the effect of coverage. First, some models with H_{1st}@M_2-N_6-graphene adsorption that is too strong or too weak were excluded (M = Sc, Ti, Fe, Zn, Y, Zr, Nb, Mo, Ag, Cd, Hf, Ta, W; the exclusion criterion was set as the absolute value of free energy greater than 0.8 eV). Under these conditions, the 1st adsorbed hydrogen atom cannot complete the formation and desorption of hydrogen gas through the Volmer–Tafel or Volmer–Heyrovsky mechanism. Next, models with H_{3rd}@M_2-N_6-graphene that are too non-spontaneous (Ni_2-N_6-graphene, Cu_2-N_6-graphene, Pd_2-N_6-graphene, W_2-N_6-graphene, Pt_2-N_6-graphene) were filtered and only their first and second hydrogen adsorption processes were analyzed. Then, the remaining models were analyzed individually:

V_2-N_6-graphene has the most favorable 1st hydrogen adsorption (+0.21 eV), followed by a decrease in the 2nd hydrogen adsorption advantage (+0.48 eV). Mn_2-N_6-graphene has similar adsorption feature to V_2-N_6-graphene. Ru_2-N_6-graphene and Au_2-N_6-graphene both have the most favorable 1st hydrogen adsorption (−0.07, +0.10 eV), followed by a decay in the 2nd hydrogen adsorption advantage (−0.97, −0.43 eV). Rh_2-N_6-graphene does not show an advantage for the 1st hydrogen adsorption (+0.59 eV), followed by an increase in the 2nd hydrogen adsorption advantage (+0.42 eV)

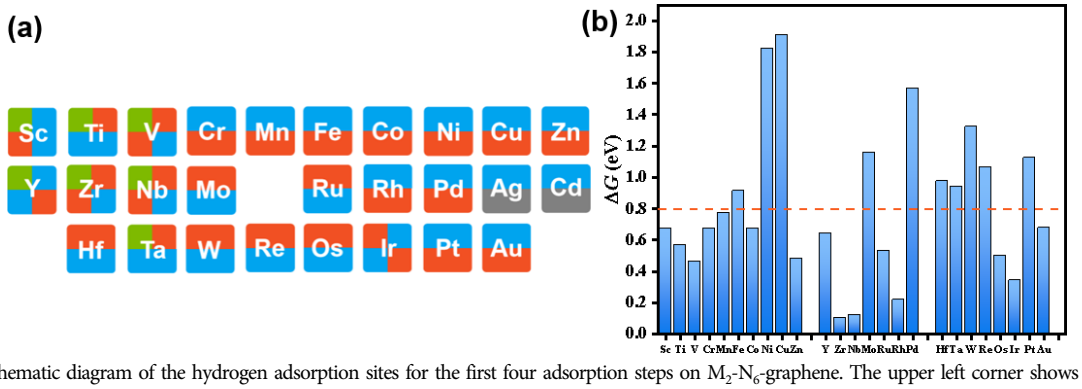

Figure 4 (a) Schematic diagram of the hydrogen adsorption sites for the first four adsorption steps on M_2-N_6-graphene. The upper left corner shows the most stable configuration for the H_{1st}@M_2-N_6-graphene; the upper right corner displays the most stable configuration for the H_{2nd}@M_2-N_6-graphene; the lower left corner illustrates the most stable configuration H_{3rd}@M_2-N_6-graphene; and the lower right corner presents the most stable configuration for the H_{4th}@M_2-N_6-graphene. Red, green, blue and yellow indicate the corresponding adsorption sites as metal top, metal-metal bridge, metal-metal shared nitrogen top and unshared nitrogen top, respectively. (b) Gibbs free energy change for the H_{3rd}@M_2-N_6-graphene site.

and then an increase in the 3rd hydrogen adsorption advantage (+0.22 eV). M_2-N_6-graphene (M = Co, Cr, Ni, Cu, Os, Pt) models have reaction free energies that vary between −0.40 and 0.40 eV for the first two hydrogen adsorptions, as shown in Fig. 5. Significantly, Pd_2-N_6-graphene has high HER activity for the second hydrogen (+0.06 eV) among the studied models and its first hydrogen adsorption is also relatively favorable (−0.46 eV). Based on thermodynamic free energy descriptors, M_2-N_6-graphene (M = Co, Cr, Ni, Cu, Ru, Pd, Os, Pt) models were selected as the potential HER candidates.

Interestingly, in these models, the adsorption sites for the first two hydrogens are the same (Fig. 4 and Fig. S20 in the ESM): the first two hydrogens adsorb on the metal top site in Ru_2-N_6-graphene and Os_2-N_6-graphene, while the first two hydrogens adsorb on the shared nitrogen-top sites in M_2-N_6-graphene (M = Cr, Co, Ni, Cu, Pd and Pt). These results emphasize that the metal-metal shared nitrogen-top sites can also be effective hydrogen adsorption sites for HER catalysts screening.

3.3 Kinetic evaluation for Tafel step

To consider the kinetic effect, the processes of generating H_2 molecule through the Tafel step in 27 M_2-N_6-graphene models were also investigated, as shown in Fig. S21 in the ESM. The barrier heights for Cr_2-N_6-graphene, Ni_2-N_6-graphene, Fe_2-N_6-graphene and Mn_2-N_6-graphene models are lower than 0.2 eV, indicating their rapid Tafel step rates. Remarkably, Fe_2-N_6-graphene shows a strong binding strength for the first hydrogen atom (ΔG_{H^*-1st} = −1.02 eV) based on thermodynamic indicators. Similarly, the Tafel step barrier in the Ir_2-N_6-graphene model is around 0.4 eV. For V_2-N_6-graphene, Co_2-N_6-graphene, Os_2-N_6-graphene, Cu_2-N_6-graphene, Au_2-N_6-graphene, Ru_2-N_6-graphene and Rh_2-N_6-graphene, the Tafel step barriers are approximately 1.0–1.4 eV. For Pd_2-N_6-graphene, Re_2-N_6-graphene, Zn_2-N_6-graphene and Pt_2-N_6-graphene, the Tafel step barriers are around 2.0 eV, which is a very slow process under normal reaction conditions.

Based on the thermodynamic screening presented above, Ni_2-N_6-graphene exhibits excellent kinetic characteristics for the Volmer–Tafel mechanism compared with Ru_2-N_6-graphene, Au_2-N_6-graphene, Os_2-N_6-graphene and Co_2-N_6-graphene. It should be highlighted that the first two hydrogen adsorption sites in Cr_2-N_6-graphene, Mn_2-N_6-graphene and Fe_2-N_6-graphene are located at shared nitrogen-top sites, while the 1st adsorption site in Ir_2-N_6-graphene is at the metal top site and the 2nd hydrogen adsorption site is at the shared nitrogen-top site (Fig. S20 in the ESM). When hydrogen on the shared nitrogen-top sites of Fe_2-N_6-graphene forms H_2 through the Volmer–Tafel mechanism, it undergoes a migration of a hydrogen atom from the shared nitrogen-top site to the metal top site firstly, as shown in Fig. 6(a), then the migrated hydrogen atom reacts with another hydrogen atom at the shared nitrogen-top site to form H_2. For Ir_2-N_6-graphene, since the distance between the two adsorbed hydrogens is close, they can react directly to form H_2 and then desorb, as shown in Fig. 6(b).

The above results indicate that the relative distance between the two adsorbed hydrogens in the Volmer–Tafel pathway may also affect the reaction barrier. Naturally, if three hydrogen atoms simultaneously adsorbed on the active region, it will result in a combination of "two metal-top sites adsorption plus one shared nitrogen-top site" or "one metal-top site adsorption plus two shared nitrogen-top sites". With increasing hydrogen coverage, H_2 can be formed from the nearby adsorbed hydrogens through the Tafel pathway. Therefore, several typical M_2-N_6-graphene (M = Cu, Ni, Co, Cr, Os, Pt, Ru) with characteristic thermodynamic behavior were selected for further study and the processes of these two hydrogens binding to form H_2 at the metal top sites and shared nitrogen sites were investigated. As shown in Fig. S24 in the ESM, it can be observed that the barrier change in Ni_2-N_6-graphene is not significant, but the overall reaction changes from endothermic to exothermic. For other models, there is a significant decay in the barriers, indicating that the combination of the adsorbed hydrogen at the metal-top site and the adsorbed hydrogen at the shared nitrogen-top site bonding to form H_2 is more favorable kinetically. From the colored diagram of the four hydrogen binding sites (Fig. 4), it can be seen that only Ir_2-N_6-graphene can form the desirable neighboring sites combination after the first two hydrogen additions, while the other models tend to form more symmetrical double metal top sites adsorption or double shared nitrogen-top sites adsorption. For these models, further increasing the coverage to form close hydrogen adsorption is crucial, but this step will be affected by the reaction free energy of the 3rd hydrogen adsorption (Fig. 4), especially for M_2-N_6-graphene (M = Cu, Ni, Pt) with high reaction free energies for the third hydrogen adsorption step. Even if increasing the coverage can effectively lower the Tafel path barrier, the high reaction free energy for the 3rd hydrogen adsorption hinders further hydrogen adsorption to these active

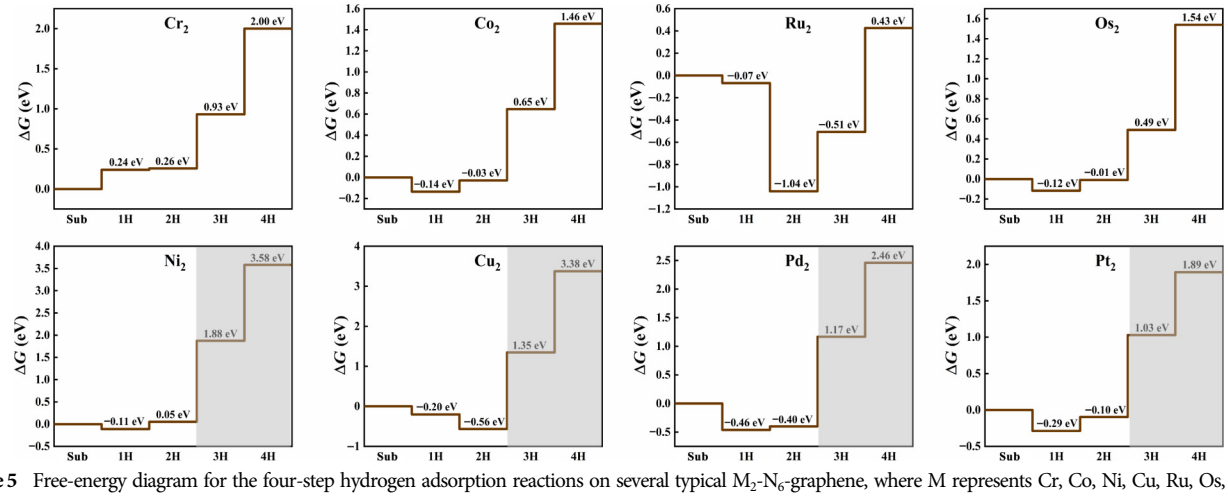

Figure 5 Free-energy diagram for the four-step hydrogen adsorption reactions on several typical M_2-N_6-graphene, where M represents Cr, Co, Ni, Cu, Ru, Os, Pd and Pt. The shadow regions indicated that the 3rd and 4th hydrogen adsorption steps were exclude.

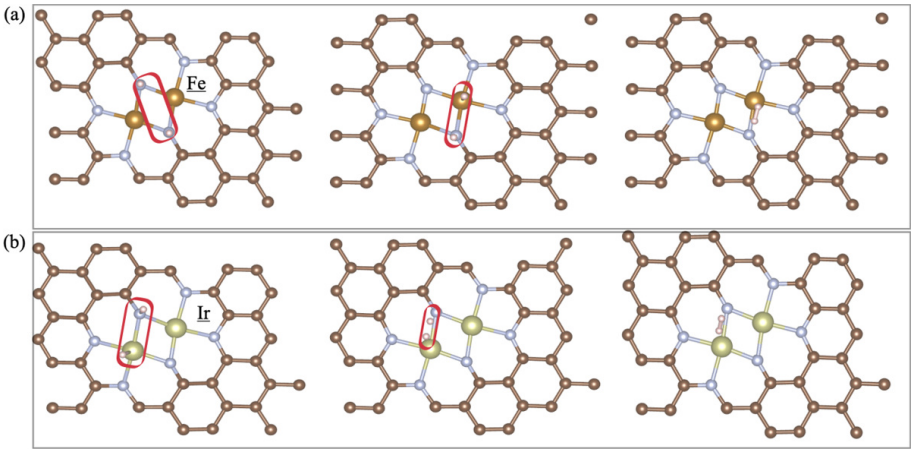

Figure 6 Selected snaps of the Tafel reaction process on (a) Fe_2-N_6-graphene and (b) Ir_2-N_6-graphene. The red circles highlight the relative positions of adsorbed hydrogen. The snaps of entire path are shown in Figs. S22 and S23 in the ESM.

centers. Therefore, for these models, the kinetic evaluation should be limited to the first two hydrogen adsorption steps.

In this section, the catalytic behavior of 27 M_2-N_6-graphene catalysts under the Volmer–Tafel mechanism was systematically investigated. The results showed that Co_2-N_6-graphene, which exhibited excellent performance in thermodynamic evaluation, had a reaction barrier of approximately 1.0 eV. This high barrier was related to the relatively far adsorption sites for the hydrogens participating in the Tafel pathway. Increasing the hydrogen coverage to make the adsorbed hydrogen at the metal top site and the adsorbed hydrogen at the shared nitrogen site participate in the Tafel pathway can significantly lower the reaction barrier. It should be emphasized that this operation of increasing hydrogen coverage is directly related to the non-spontaneous reaction free energy of the third hydrogen adsorption. Based on kinetic descriptors, M_2-N_6-graphene (M = Co, Cr) models were selected as the potential HER candidates.

3.4 Kinetic evaluation for water dissociation

Considering the water dissociation step in HER is necessary to capture the complete mechanism, especially in acidic or near-neutral conditions. It makes catalyst performance evaluation more accurate and facilitates a better comparison with experimental data. Herein, we focused on studying the water dissociation reaction for 11 representative M_2-N_6-graphene models containing Co, Cr, Cu, Fe, Ir, Mn, Ni, Os, Pt, Zn and Ru. The distance between the water molecule and the substrate on Cr_2-N_6-graphene after geometry optimization is 2.10 Å (210 pm), which is longer than the sum of the radii of the two atoms (118 pm + 66 pm = 184 pm). For the other 10 models, there is a significant physical adsorption feature: the hydrogen atom in the water molecule points towards the M_2-N_6 region of the substrate and the distance between the water molecule and the substrate is around 3.00 Å (Fig. S25 in the ESM). Two possible dissociation configurations were considered: in the first dissociation mode, each metal top site adsorbs a hydroxide ion (OH^-) and a proton (H^+), respectively. In the second dissociation mode, one metal top site adsorbs OH^- and the shared nitrogen-top site adsorbs H^+ (Figs. S26 and S27 in the ESM). Interestingly, Cu_2-N_6-graphene and Ni_2-N_6-graphene cannot form these two dissociation configurations. This result indicates that Cu_2-N_6-graphene and Ni_2-N_6-graphene have lower activity in the water dissociation reaction, which means that in alkaline environments, water molecules as a hydrogen source are less likely to undergo HER reactions on Cu_2-N_6-graphene and Ni_2-N_6-graphene. M_2-N_6-graphene containing metals Cr, Os, Ru, Fe and Mn prefers to dissociate the water molecule as the first dissociation mode. Meanwhile, M_2-N_6-graphene containing metals Co, Pt, Zn and Ir prefers to dissociate the water molecule as the second dissociation mode. Based on the NEB method, the corresponding dissociation reaction pathways were obtained, as shown in Fig. S28 in the ESM. It is worth noting that most dissociation reactions are endothermic in thermodynamics. However, the second dissociation mode in Zn_2-N_6-graphene and the first dissociation mode in Cr_2-N_6-graphene are exothermic reactions. For Cr_2-N_6-graphene, as mentioned earlier, this is due to the relatively tight binding between Cr–O during molecular adsorption. For Zn_2-N_6-graphene, after forming the second dissociation mode, a significant deformation occurs in the Zn-N-H region. N–H is basically in the same plane as the substrate. The embedded H atom cannot act as a favorable intermediate structure for HER (Fig. S29 in the ESM). It can be judged that Zn_2-N_6-graphene is not suitable for use as an alkaline HER catalyst.

For the remaining models, the more energies needed during the dissociation reaction, the higher of barrier needed to be overcome. For example, reaction energy is higher when water dissociated on the double metal sites of Co_2-N_6-graphene than the reaction energy when water dissociated on the metal top site and shared nitrogen-top site. Meanwhile, the barrier height for the first dissociation method is also higher than that for the second method (2.0 vs. 1.5 eV). In summary, only four water dissociation barriers on Cr_2-N_6-graphene, Ru_2-N_6-graphene and Mn_2-N_6-graphene are less than 1.0 eV, as shown in Fig. 7. It should be mentioned that the first hydrogen prefers to occupy metal top site and shared nitrogen-top site on Ru_2-N_6-graphene and Mn_2-N_6-graphene, respectively. The sites consistent between first hydrogen adsorption and water dissociation produced proton occupation suggested that Cr and Ru play a special role in this double metal site and when designing hetero-dual atomic site M_aM_b-N_6-graphene for subsequent alkaline HER, one of the sites should be optimally selected as non-noble Cr atom to achieve higher screening efficiency.

4 Conclusion

In summary, based on the thermodynamic and kinetic perspectives, this paper provides an evaluation of the HER catalytic performance

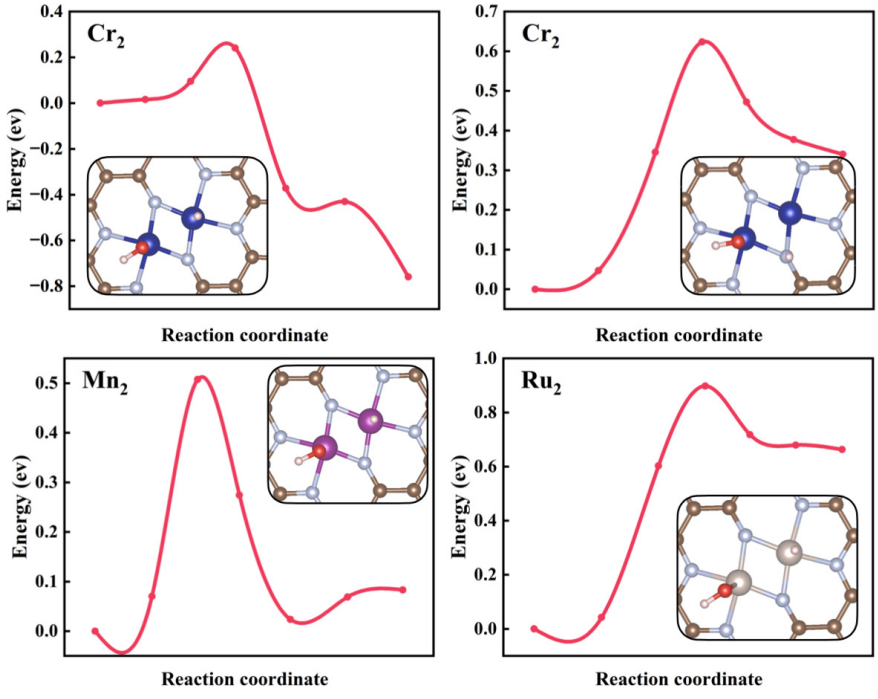

Figure 7 Water dissociation pathways on the M_2-N_6-graphene substrate with energy barriers lower than 1.0 eV.

of 27 homo-M_2-N_6-graphene models. The structural research shows that the reaction free energy of the 1st hydrogen adsorption step can be used for rapid screening of extreme cases, but may lead to significant evaluation bias, so the steps involved in HER should be carefully examined and multiple indicators should be used for evaluation and screening. In addition, the shared nitrogen site is also an important type of hydrogen adsorption reaction site in this system and this type of position should be focused on in future research on similar catalytic mechanisms for this model. The activity evaluation of HER should consider the impact of hydrogen coverage and the relative distance between hydrogen adsorption sites will directly affect the reaction barrier of the Tafel step. Thermodynamic and kinetic indicators will form mutually restricting conditions, for example, in this system, the change in the reaction free energy of the third hydrogen adsorption step, a non-spontaneous step, determines the upper limit of the coverage. If designing hetero-M_aM_b-N_6-graphene models for HER catalysts, introducing V elements can improve screening efficiency. If designing hetero-M_aM_b-N_6-graphene models for HER alkaline catalysts, one of the sites should be optimally selected as Cr atom, i.e., CrM-N_6-graphene and when screening for the second metal atom, Cu and Ni elements should be discarded to greatly improve the screening efficiency.

This work initially establishes a HER performance evaluation process: first, screen for metals and potential hydrogen adsorption sites near them, complete the calculation of the reaction free energy of the first hydrogen adsorption step and exclude extreme cases based on the Sabatier principle (ΔG_{H^*} with an absolute value greater than 1.0 eV); second, increase the hydrogen adsorption coverage to occupy the 2nd adsorption site, the 3rd, or even the 4th adsorption site, calculate the reaction free energy for each step of hydrogen adsorption, find the characteristic non-spontaneous adsorption steps and complete the thermodynamic indicator evaluation; third, based on the dynamic energy barrier of the Tafel step under consideration of multiple adsorption sites, exclude models that are difficult to perform dynamically (reaction barrier greater than 1.0 eV); fourth, according to energy barrier needed to overcome, examine whether the water dissociation process can occur and whether the dissociated H* is bonded to the optimal adsorption site determined in the first step and classify it for its acid-base application environment.

Electronic Supplementary Material: Supplementary material (Figs. S1–S29 and Table S1) is available in the online version of this article at https://doi.org/10.26599/NR.2025.94907004.

Data availability

All data needed to support the conclusions in the paper are presented in the manuscript and/or the Electronic Supplementary Material. Additional data related to this paper may be requested from the corresponding author upon request.

Acknowledgements

This work was supported by the National Natural Science Foundation of China (No. 22101029), Beijing Natural Science Foundation (No. 2222006) and Beijing Municipal Financial Project BJAST Young Scholar Programs B (No. YS202202). The authors acknowledge computational resources of "TianHe-1A" supercomputer at the National Supercomputing Center in Tianjin and technical support from TianHe Supercomputing Center of Huaihai.

Declaration of competing interest

All the contributing authors report no conflict of interests in this work.

Author contribution statement

J. M.: Conceptualization, data curation, writing – original draft. L.

T. F.: Data curation, validation, writing– original draft. Z. Y. Z.: Methodology, software, visualization. L. Z.: Resources, project administration. X. W. L.: Funding acquisition, writing – review & editing, supervision. Z. W. Z.: Supervision, writing – review & editing. W. M. S.: Conceptualization, supervision, writing – review & editing. All authors have read and approved the final manuscript.

Use of AI statement

None.

References

[1] Chu, S.; Majumdar, A. Opportunities and challenges for a sustainable energy future. *Nature* **2012**, *488*, 294–303.

[2] Chen, C. L.; Sun, M. Z.; Zhang, F.; Li, H. J.; Sun, M. R.; Fang, P.; Song, T. L.; Chen, W. X.; Dong, J. C.; Rosen, B. et al. Adjacent Fe site boosts electrocatalytic oxygen evolution at Co site in single-atom-catalyst through a dual-metal-site design. *Energy Environ. Sci.* **2023**, *16*, 1685–1696.

[3] Hu, Y. F.; Li, Z. S.; Li, B. L.; Yu, C. L. Recent progress of diatomic catalysts: General design fundamentals and diversified catalytic applications. *Small* **2022**, *18*, 2203589.

[4] Sun, F.; Tang, Q.; Jiang, D. E. Theoretical advances in understanding and designing the active sites for hydrogen evolution reaction. *ACS Catal.* **2022**, *12*, 8404–8433.

[5] Zhu, Y. M.; Klingenhof, M.; Gao, C. L.; Koketsu, T.; Weiser, G.; Pi, Y. C.; Liu, S. H.; Sui, L. J.; Hou, J. R.; Li, J. Y. et al. Facilitating alkaline hydrogen evolution reaction on the hetero-interfaced Ru/RuO_2 through Pt single atoms doping. *Nat. Commun.* **2024**, *15*, 1447.

[6] Barlocco, I.; Di Liberto, G.; Pacchioni, G. Hydrogen and oxygen evolution reactions on single atom catalysts stabilized by a covalent organic framework. *Energy Adv.* **2023**, *2*, 1022–1029.

[7] Zhang, T. Y.; Jin, J.; Chen, J. M.; Fang, Y. Y.; Han, X.; Chen, J. Y.; Li, Y. P.; Wang, Y.; Liu, J. F.; Wang, L. Pinpointing the axial ligand effect on platinum single-atom-catalyst towards efficient alkaline hydrogen evolution reaction. *Nat. Commun.* **2022**, *13*, 6875.

[8] Yao, R.; Sun, K. A.; Zhang, K. Y.; Wu, Y.; Du, Y. J.; Zhao, Q.; Liu, G.; Chen, C.; Sun, Y. H.; Li, J. P. Stable hydrogen evolution reaction at high current densities via designing the Ni single atoms and Ru nanoparticles linked by carbon bridges. *Nat. Commun.* **2024**, *15*, 2218.

[9] Wang, C.; Zang, H.; Liu, C. J.; Wang, J. H.; Kuai, L.; Geng, B. Y. Synergistic acid hydrogen evolution of neighboring Pt single atoms and clusters: Understanding their superior activity and mechanism. *Inorg. Chem.* **2023**, *62*, 6856–6863.

[10] Guan, S. Y.; Yuan, Z. L.; Zhuang, Z. C.; Zhang, H. H.; Wen, H.; Fan, Y. P.; Li, B. J.; Wang, D. S.; Liu, B. Z. Why do single-atom alloys catalysts outperform both single-atom catalysts and nanocatalysts on mxene. *Angew. Chem., Int. Ed.* **2024**, *63*, e202316550.

[11] Hu, Y. M.; Chao, T. T.; Li, Y. P.; Liu, P. G.; Zhao, T. H.; Yu, G.; Chen, C.; Liang, X.; Jin, H. L.; Niu, S. W. et al. Cooperative Ni(Co)-Ru-P sites activate dehydrogenation for hydrazine oxidation assisting self-powered H_2 production. *Angew. Chem., Int. Ed.* **2023**, *62*, e202308800.

[12] Guan, S. Y.; Yuan, Z. L.; Zhao, S. Q.; Zhuang, Z. C.; Zhang, H. H.; Shen, R. F.; Fan, Y. P.; Li, B. J.; Wang, D. S.; Liu, B. Z. Efficient hydrogen generation from ammonia borane hydrolysis on a tandem ruthenium-platinum-titanium catalyst. *Angew. Chem., Int. Ed.* **2024**, *63*, e202408193.

[13] Li, Y. P.; Niu, S. W.; Liu, P. G.; Pan, R. R.; Zhang, H. K.; Ahmad, N.; Shi, Y.; Liang, X.; Cheng, M. Y.; Chen, S. H. et al. Ruthenium nanoclusters and single atoms on α-MoC/N-doped carbon achieves low-input/input-free hydrogen evolution via decoupled/coupled hydrazine oxidation. *Angew. Chem., Int. Ed.* **2024**, *63*, e202316755.

[14] Zhu, P.; Xiong, X.; Wang, D. S. Regulations of active moiety in single atom catalysts for electrochemical hydrogen evolution reaction. *Nano Res.* **2022**, *15*, 5792–5815.

[15] Zheng, X. B.; Li, B. B.; Wang, Q. S.; Wang, D. S.; Li, Y. D. Emerging low-nuclearity supported metal catalysts with atomic level precision for efficient heterogeneous catalysis. *Nano Res.* **2022**, *15*, 7806–7839.

[16] Jing, H. Y.; Zhu, P.; Zheng, X. B.; Zhang, Z. D.; Wang, D. S.; Li, Y. D. Theory-oriented screening and discovery of advanced energy transformation materials in electrocatalysis. *Adv. Powder Mater.* **2022**, *1*, 100013.

[17] Li, R. Z.; Wang, D. S. Understanding the structure–performance relationship of active sites at atomic scale. *Nano Res.* **2022**, *15*, 6888–6923.

[18] Tang, B.; Zhou, Y. N.; Ji, Q. Q.; Zhuang, Z. C.; Zhang, L.; Wang, C.; Hu, H. B.; Wang, H. J.; Mei, B. B.; Song, F. et al. A janus dual-atom catalyst for electrocatalytic oxygen reduction and evolution. *Nat. Synth.* **2024**, *3*, 878–890.

[19] Zhu, P.; Xiong, X.; Wang, D. S.; Li, Y. D. Advances and regulation strategies of the active moiety in dual-atom site catalysts for efficient electrocatalysis. *Adv. Energy Mater.* **2023**, *13*, 2300884.

[20] Tian, S. B.; Wang, B. X.; Gong, W. B.; He, Z. Z.; Xu, Q.; Chen, W. X.; Zhang, Q. H.; Zhu, Y. Q.; Yang, J. R.; Fu, Q. et al. Dual-atom Pt heterogeneous catalyst with excellent catalytic performances for the selective hydrogenation and epoxidation. *Nat. Commun.* **2021**, *12*, 3181.

[21] Tang, M. H.; Shen, J.; Wang, Y. D.; Zhao, Y. F.; Gan, T.; Zheng, X. S.; Wang, D. S.; Han, B. X.; Liu, Z. M. Highly efficient recycling of polyester wastes to diols using Ru and Mo dual-atom catalyst. *Nat. Commun.* **2024**, *15*, 5630.

[22] Fang, C.; Zhou, J.; Zhang, L. L.; Wan, W. C.; Ding, Y. X.; Sun, X. Y. Synergy of dual-atom catalysts deviated from the scaling relationship for oxygen evolution reaction. *Nat. Commun.* **2023**, *14*, 4449.

[23] Zhu, P.; Xiong, X.; Wang, X. L.; Ye, C. L.; Li, J. Z.; Sun, W. M.; Sun, X. H.; Jiang, J. J.; Zhuang, Z. B.; Wang, D. S. et al. Regulating the FeN_4 moiety by constructing Fe-Mo dual-metal atom sites for efficient electrochemical oxygen reduction. *Nano Lett.* **2022**, *22*, 9507–9515.

[24] Li, R. Z.; Wang, D. S. Superiority of dual-atom catalysts in electrocatalysis: One step further than single-atom catalysts. *Adv. Energy Mater.* **2022**, *12*, 2103564.

[25] Mu, X. Q.; Liu, S. L.; Zhang, M. Y.; Zhuang, Z. C.; Chen, D.; Liao, Y. R.; Zhao, H. Y.; Mu, S. C.; Wang, D. S.; Dai, Z. H. Symmetry-broken Ru nanoparticles with parasitic Ru-Co dual-single atoms overcome the Volmer step of alkaline hydrogen oxidation. *Angew. Chem., Int. Ed.* **2024**, *63*, e202319618.

[26] Chen, Y.; Lin, J.; Pan, Q.; Liu, X.; Ma, T. Y.; Wang, X. D. Inter-metal interaction of dual-atom catalysts in heterogeneous catalysis. *Angew. Chem., Int. Ed.* **2023**, *62*, e202306469.

[27] Gong, Y. N.; Cao, C. Y.; Shi, W. J.; Zhang, J. H.; Deng, J. H.; Lu, T. B.; Zhong, D. C. Modulating the electronic structures of dual-atom catalysts via coordination environment engineering for boosting CO_2 electroreduction. *Angew. Chem., Int. Ed.* **2022**, *61*, e202215187.

[28] Wang, Y.; Park, B. J.; Paidi, V. K.; Huang, R.; Lee, Y.; Noh, K. J.; Lee, K. S.; Han, J. W. Precisely constructing orbital coupling-modulated dual-atom Fe pair sites for synergistic CO_2 electroreduction. *ACS Energy Lett.* **2022**, *7*, 640–649.

[29] Levell, Z.; Le, J. B.; Yu, S.; Wang, R. Y.; Ethirajan, S.; Rana, R.; Kulkarni, A.; Resasco, J.; Lu, D. Y.; Cheng, J. et al. Emerging atomistic modeling methods for heterogeneous electrocatalysis. *Chem. Rev.* **2024**, *124*, 8620–8656.

[30] Kumar, A.; Bui, V. Q.; Lee, J.; Wang, L. L.; Jadhav, A. R.; Liu, X. H.; Shao, X. D.; Liu, Y.; Yu, J. M.; Hwang, Y. et al. Moving beyond bimetallic-alloy to single-atom dimer atomic-interface for all-pH

hydrogen evolution. *Nat. Commun.* **2021**, *12*, 6766.

[31] Zhang, L. H.; Guo, X. Y.; Zhang, S. L.; Huang, S. P. Building up the "genome" of bi-atom catalysts toward efficient HER/OER/ORR. *J. Mater. Chem. A* **2022**, *10*, 11600–11612.

[32] Nørskov, J. K.; Rossmeisl, J.; Logadottir, A.; Lindqvist, L.; Kitchin, J. R.; Bligaard, T.; Jónsson, H. Origin of the overpotential for oxygen reduction at a fuel-cell cathode. *J. Phys. Chem. B* **2004**, *108*, 17886–17892.

[33] Fei, H. L.; Dong, J. C.; Feng, Y. X.; Allen, C. S.; Wan, C. Z.; Volosskiy, B.; Li, M. F.; Zhao, Z. P.; Wang, Y. L.; Sun, H. T. et al. General synthesis and definitive structural identification of MN_4C_4 single-atom catalysts with tunable electrocatalytic activities. *Nat. Catal.* **2018**, *1*, 63–72.

[34] Li, R. Z.; Zhang, Z. D.; Liang, X.; Shen, J.; Wang, J.; Sun, W. M.; Wang, D. S.; Jiang, J. C.; Li, Y. D. Polystyrene waste thermochemical hydrogenation to ethylbenzene by a N-bridged Co, Ni dual-atom catalyst. *J. Am. Chem. Soc.* **2023**, *145*, 16218–16227.

[35] Meng, X. B.; Zhao, Z. Q.; Li, K.; Liu, Y. W.; Sun, W. M.; Zhai, T. Y.; Lin, Y. Q. Neighboring V atom as a catalytic switch: Reversing the active site for exceptional water splitting. *Appl. Catal. B: Environ. Energy* **2024**, *351*, 123942.

[36] Giannozzi, P.; Baroni, S.; Bonini, N.; Calandra, M.; Car, R.; Cavazzoni, C.; Ceresoli, D.; Chiarotti, G. L.; Cococcioni, M.; Dabo, I. et al. Quantum ESPRESSO: A modular and open-source software project for quantum simulations of materials. *J. Phys.: Condens. Matter.* **2009**, *21*, 395502.

[37] Giannozzi, P.; Andreussi, O.; Brumme, T.; Bunau, O.; Buongiorno Nardelli, M.; Calandra, M.; Car, R.; Cavazzoni, C.; Ceresoli, D.; Cococcioni, M. et al. Advanced capabilities for materials modelling with quantum ESPRESSO. *J. Phys.: Condens. Matter.* **2017**, *29*, 465901.

[38] Perdew, J. P.; Burke, K.; Ernzerhof, M. Generalized gradient approximation made simple. *Phys. Rev. Lett.* **1996**, *77*, 3865–3868.

[39] Garrity, K. F.; Bennett, J. W.; Rabe, K. M.; Vanderbilt, D. Pseudopotentials for high-throughput DFT calculations. *Comput. Mater. Sci.* **2014**, *81*, 446–452.

[40] Wang, L.; Maxisch, T.; Ceder, G. Oxidation energies of transition metal oxides within the GGA + *U* framework. *Phys. Rev. B.* **2006**, *73*, 195107.

[41] Xu, H. X.; Cheng, D. J.; Cao, D. P.; Zeng, X. C. Retracted article: A universal principle for a rational design of single-atom electrocatalysts. *Nat. Catal.* **2018**, *1*, 339–348.

[42] Marzari, N.; Vanderbilt, D.; De Vita, A.; Payne, M. C. Thermal contraction and disordering of the Al (110) surface. *Phys. Rev. Lett.* **1999**, *82*, 3296–3299.

[43] Skúlason, E.; Tripkovic, V.; Björketun, M. E.; Gudmundsdóttir, S.; Karlberg, G.; Rossmeisl, J.; Bligaard, T.; Jónsson, H.; Nørskov, J. K. Modeling the electrochemical hydrogen oxidation and evolution reactions on the basis of density functional theory calculations. *J. Phys. Chem. C* **2010**, *114*, 18182–18197.

[44] Di Liberto, G.; Cipriano, L. A.; Pacchioni, G. Universal principles for the rational design of single atom electrocatalysts. *Handle with care. ACS Catal.* **2022**, *12*, 5846–5856.